Available online at www.sciencedirect.com
ScienceDirect
Ceramics International 36 (2010) 275–281
CERAMICS INTERNATIONAL
www.elsevier.com/locate/ceramint

Structural and magnetic phase evolution study on needle-shaped nanoparticles of magnesium ferrite

T.K. Pathak, N.H. Vasoya, V.K. Lakhani, K.B. Modi *

Department of Physics, Saurashtra University, Rajkot 360 005, India

Received 18 June 2009; received in revised form 2 July 2009; accepted 27 July 2009
Available online 25 August 2009

Abstract

Nanoparticles of magnesium ferrite ($MgFe_2O_4$) have been synthesized by chemical co-precipitation route. The microstructure, infrared spectral and magnetic properties have been studied by means of X-ray diffraction, transmission electron microscopy, thermogravimetric analysis, infrared spectroscopy, high field magnetization, low field ac susceptibility and Mossbauer spectroscopic measurements. Transmission electron microscopy (TEM) observation showed that the nanocrystals present a needle-like shape with an aspect ratio of around 3.5 and long axis of 37 nm. The kinetics of needle-shaped nanocrystals formation has been discussed. The Mg^{2+} seems to play key role in governing the rate of growth of growing planes of nanocrystals. The magnetic behaviour is explained by invoking the concept of super-paramagnetism assuming core–shell structure of the nanoparticles. Mossbauer spectral and susceptibility studies showed that the as-prepared nano-sized ferrite is super paramagnetic at room temperature and magnetic ordering evolves on baking and annealing the nanopowdered sample due to increase in the crystalline size. The high temperature annealing transforms the nanostructured ferrite to ordered magnetic structure of ceramic ferrite having long range ferrimagnetic ordering. Infrared (IR) spectral analysis reveals the weak high frequency shoulder due to disparity in the masses of cations present at tetrahedral sites, while splitting of low and high frequency absorption bands has been explained on the basis of Jahn–Teller effect in Fe^{2+}-ions which lead to a non-cubic component of the crystal field potential.

Keywords: A. Powders: chemical preparation; B. Grain size; C. Magnetic properties; D. Ferrites

1. Introduction

The research in nano-science can be framed with three aims: to synthesize, understand and explore new nano-materials and the related phenomena. Nanoparticles of spinel ferrites are of great interest in fundamental science for addressing relationship between physical properties and their crystal chemistry and structure. Due to their reduced sizes, these nanoparticles may possess novel and/or improved properties in comparison to the bulk materials. This has renewed interest to study different properties of pure and mixed spinel ferrite systems in nanocrystalline regime. A wide variety of techniques are being used to synthesize nanos-tructured materials including gas condensation, rapid solidi-fication, electrodeposition, sputtering, crystallization of amorphous phases [1], wet-chemical methods like co-precipitation, sonochemical reactions, sol–gel method, com-bustion, reverse micelle technique, hydrothermal route [2–8] and mechanical attrition-ball milling [9–11].

Magnesium ferrite ($MgFe_2O_4$) is a partially inverse spinel and its degree of inversion is sensitive to the thermal history of the sample, microstructure and preparative parameters. More importantly, it has been shown that shape of nanoparticles strongly influences the magnetic properties and the coercive force of needle-shaped particles is generally higher than that of their isometric counterparts [12,13]. Furthermore, it has been shown that specific surface area of needle-shaped nanoparticles is greater than lamellar or rod-shaped particles [14]. In the field of nano-magnetism this surface area plays very important role in governing magnetic properties. The present work deals with the synthesis of $MgFe_2O_4$ nanoparticles using chemical co-precipitation, study of their structural and magnetic properties and the change in its properties due to heat treatment given to the material.

* Corresponding author. Tel.: +91 281 2588428; fax: +91 281 2577633.
E-mail address: kunalbmodi2003@yahoo.com (K.B. Modi).

0272-8842/$36.00
doi:10.1016/j.ceramint.2009.07.023

2. Experimental details

The spinel ferrite, $MgFe_2O_4$, was prepared by air oxidation of an aqueous suspension containing Mg^{2+} and Fe^{2+} cations in stoichiometric proportions. The starting solutions were prepared by mixing 50 ml of aqueous solutions of $MgSO_4{\cdot}7H_2O$ and $FeSO_4{\cdot}7H_2O$ in proper proportions. A 2 M solution of NaOH was prepared as a precipitant. The starting solution (pH ~3.5) was added into the precipitant because the solubility product constants for the hydroxides of the cation are exceeded and sequential precipitation of the hydroxides can be avoided. The suspension (pH 10.5) containing dark green intermediate precipitates was formed. Then the suspension was heated and kept at 60 °C temperature, while hydrogen peroxide (H_2O_2) was added to promote oxidation reaction until all the intermediate precipitates changed into the dark brownish precipitates of the spinel ferrite. The sample was filtered, washed by acetone and dried at 100 °C under vacuum (wet sample). To study the structural and magnetic phase evolution one set of the wet sample (as prepared) was baked at 400 °C for 6 h while other set of sample was sintered in air at 1100 °C for 18 h and slowly cooled to room temperature (annealed sample). The stoichiometry of the powdered sample was checked by energy dispersive analysis of X-rays (EDAX). The compositional values were determined within the accuracy of 1%. X-ray diffraction data were collected on a Philips PW 1710 automated X-ray powder diffractometer using Cu Kα radiation, graphite monochromator, and Xe-filled proportional counter. Data were collected in the angle range 5–90°. Microstructural characterization was performed by transmission electron microscopy (TEM), using a TECNAIK20 (Philips) microscope operated at 200 kV. For the TEM observations, the powder was first dispersed in amyl acetate by ultrasonication and then the suspension was dropped on a copper grid with a carbon film. The thermogravimetric analysis (TGA) was carried out on Pyrif-1, PerkinElmer, in the atmosphere of air from 50 °C to 500 °C at a heating rate of 10 °C/min. For recording IR spectrum, powder was mixed with KBr in the ratio 1:100 by weight to ensure uniform dispersion in the KBr pellet. The mixed powder was then pressed in a cylindrical die to obtain clear disc. The IR spectrum in the wave number range 400–4000 cm^{-1} was recorded at 300 K on PerkinElmer made IR spectrometer. The saturation magnetization measurements of samples were carried out using high field (4 kOe) hysteresis loop technique [15] at 80 K. The ac susceptibility measurements on powdered samples were made in the temperature range 300–750 K using a double coil set up [16] operating at a frequency of 263 Hz and in r.m.s. field of 0.5 Oe. Mossbauer spectrometer of electro mechanical type was used, in the constant acceleration mode, to obtain the spectra of the samples at 300 K, in the transmission mode. A 10 mCi: ^{50}Co source in rhodium matrix was used where the absorber thickness was ideally thin. It is quite possible that the nature of the sample will be continuously changing when the sample temperature increases beyond preparation temperature but our main objectives in this work were to determine Neel temperature of the samples and to see the collective response of particles of various size at different temperatures.

3. Results and discussion

The room temperature (300 K) X-ray diffraction (XRD) pattern for wet sample of magnesium ferrite is shown in Fig. 1. The Bragg reflections (3 1 1), (4 0 0), (3 3 3) and (4 4 0) are conspicuous and are correspond to spinel structure, while the other reflections are comparatively weak. The background noise and broadness of the peaks are characteristic of particles with nanometer dimensions. This happens because in the nano-sized particles there are insufficient diffraction centers that cause the line broadening.

The XRD pattern of annealed sample shows sharp Bragg reflections corresponding to the fcc spinel structure; thus exhibiting no signature of evolution of any extra phase after high temperature annealing; confirming good quality of wet-prepared ferrite sample with expected stoichiometry. The sharp Bragg reflection indicates that the fine particle nature is lost due to high temperature annealing and the ferrite material is akin to the coarse grained ceramically prepared product.

The average particle size or thickness of the crystal (D) for wet-chemically synthesized $MgFe_2O_4$ was determined from the broadening of the respective high intensity (3 1 1) peak using

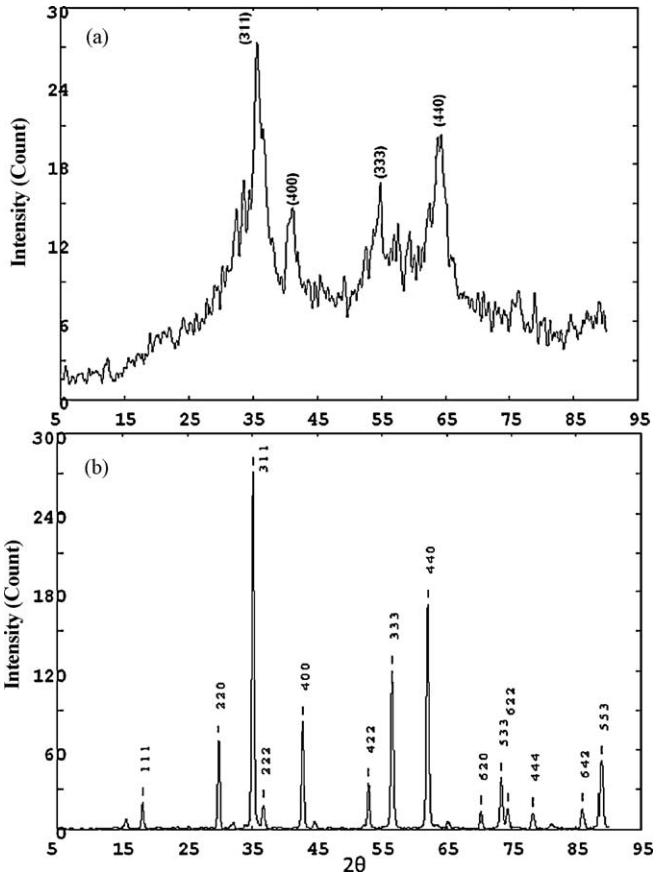

Fig. 1. X-ray diffraction patterns for wet sample (a) and annealed sample (b) of $MgFe_2O_4$ at 300 K.

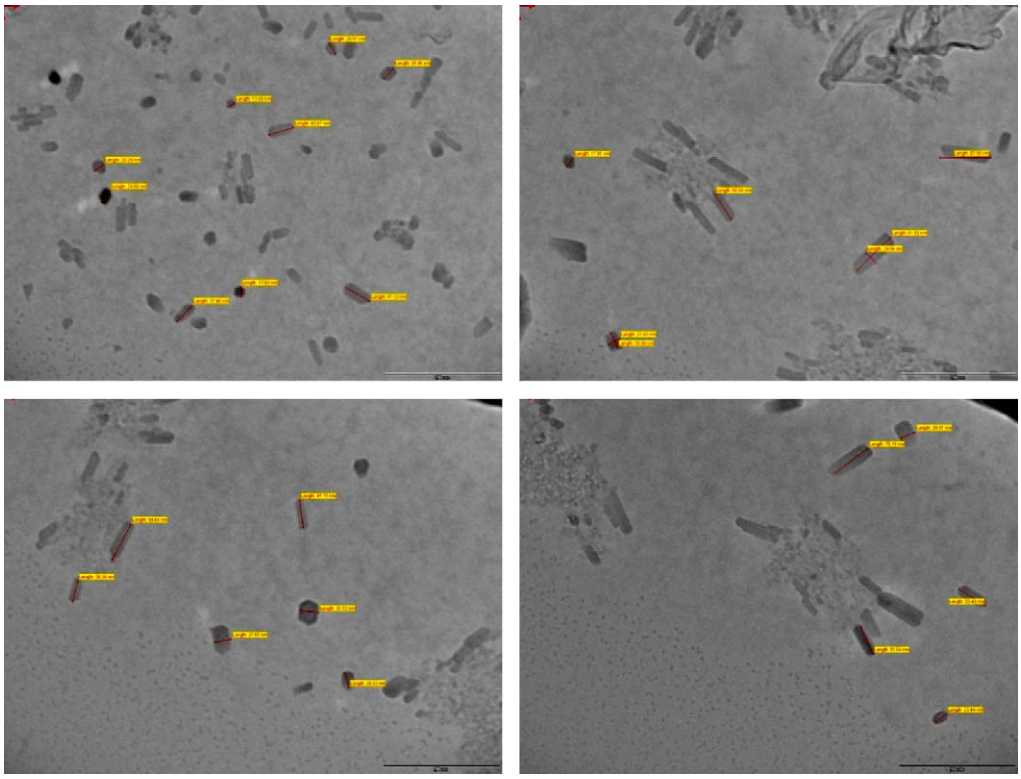

Fig. 2. TEM images for nanocrystalline magnesium ferrite.

the Debye Scherrer's formula [17]:

$$D = \frac{K\lambda}{B\cos\theta}$$

Here, λ is the wave length of the Cu Kα radiation (=0.15418 nm), constant K (=0.9) is related both to the crystallite shaped and the way in which B and D are defined. B is the contribution to the XRD peak width due to the small size of crystallites in radians. The contribution must separate out from the measured line width B_M which includes instrumental broadening b, always parent irrespective of the particle size, for this one can record XRD pattern of a well crystallized, bulk standard material such as silicon powder under identical geometrical condition and measure the peak width b (=0.08° = 1.3955×10^{-3} radian is taken). The broadening parameter B is obtained from the relation:

$$B = (B_M^2 - b^2)^{1/2}$$

The average particle size is found to be ∼26 nm. The particle size when calculated at different Bragg angle values, was found to remain unaltered, indicating the absence of strain.

The X-ray diffraction (XRD) pattern analysis reveals the crystal structure, crystal parameters and average crystalline size, while transmission electron microscopy (TEM) shows the particle morphology and its size distribution. XRD gives the average crystalline size and no clue about its distribution. On the other hand, TEM can be used to measure the particle size of individual particles, which is one of the most basic parameters in nanoparticle research. That can then be used to quantitively look at the particle size distribution in the sample. Also, if there are more than one phases in the sample that can be revealed by using XRD and TEM results.

Typically TEM images for magnesium ferrite are shown in Fig. 2. It can be seen that the particles are quite well dispersed and not much agglomerations are present. They reveal that the obtained ferrites are thick needle-shaped (acicular) nanocrystals with an aspect ratio of around 3.5 and a average long axis of 37 nm. We have also observed very few nanoparticles of distorted hexagonal morphology.

The particle size estimated from TEM is slightly greater than the particle size estimated from XRD using Scherrer's formula. This is because X-ray diffraction gives the information of crystalline region only and the contribution from the amorphous grain surface does not contribute. On the other hand TEM gives the complete picture of the nanoparticles. By analyzing TEM and XRD one can have almost complete picture of the particle size, their distribution and morphology.

Recently, it has been reported by Cao and Gu [4] that the smooth decomposition of urea and the resulting co-precipitation in oleic acid micelles lead to needle-shaped nanocrystals on a large scale. On the other hand Qu et al. [14] have shown that reaction temperature, reactant concentration and alkaline injecting rate are crucial factors in determining the morphologies of the nanoparticle while Moon et al. [18] have suggested that the presence and addition sequence of hydrogen peroxide significantly influence particle characteristics. It has been demonstrated by Khunti et al. [19] that the Mg^{2+} plays important role to change morphology of calcite crystals from rhombohedral to complicated floral type or bunch type in the sea water.

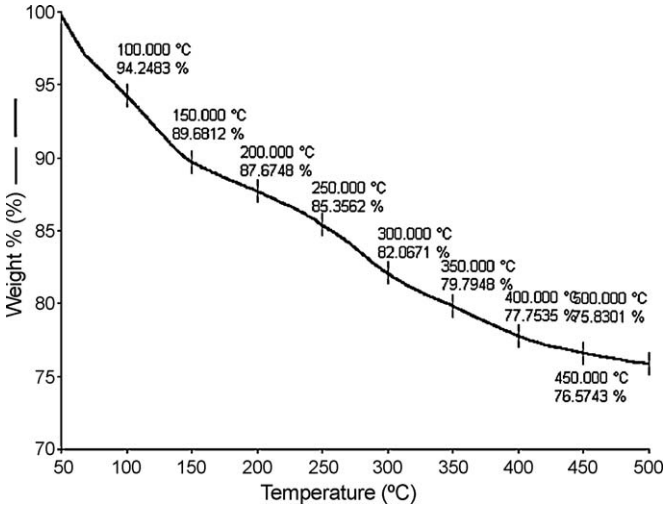

Fig. 3. TGA curve for nanocrystalline $MgFe_2O_4$.

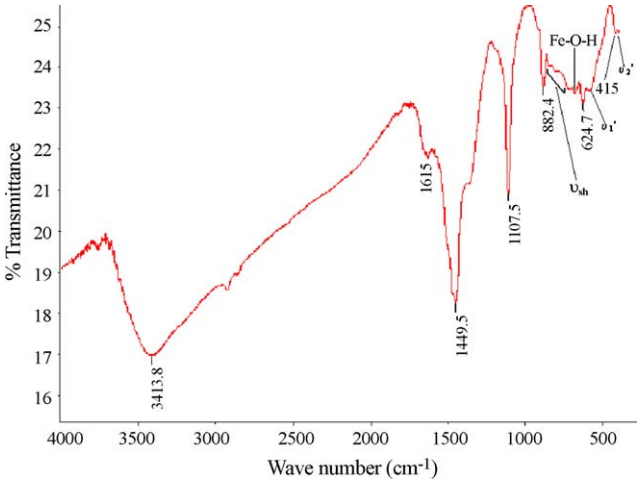

Fig. 4. Infrared spectrum of nanocrystalline $MgFe_2O_4$ at 300 K.

It is well know that materials with a cubic crystal structure are prone to grow into a spherical shape [2–3,20] to minimize the surface tension. Based on above studies, mechanism for the formation of needle-shaped nanoparticles of $MgFe_2O_4$ can be explained as follows. In the present case strong alkaline solution, sodium hydroxide (NaOH) used as a precipitant smoothly liberate hydroxide ions, that would retard the nucleation and growth rate of nanocrystals which is advantageous for the growth of one-dimensional (1D) structures. On the other hand hydrogen peroxide (H_2O_2) used as a oxidizing agent and Mg^{2+} ions altered the surface tension of the growing crystal and the growth rate of the nanocrystal along the bound crystal planes is slowed down or stopped [21,22], resulting in the formation of needle-like nanocrystals.

Thermogravimetry is the measurement of the mass of a sample as the temperature increase. This method is useful for determining sample purity and water, carbonate and organic content, and for studying decomposition reaction. TGA curve for wet sample of magnesium ferrite is shown in Fig. 3. TGA curve shows continue weight loss on heating. The observed weight loss is due to desorption of water and removal of organic impurity if any, from the sample. The net weight loss is found to be ∼24% in the temperature range studied and the maximum weight loss takes place before 200 °C.

Ferrite possesses the structure of mineral spinel ($MgAl_2O_4$) that crystallized in the cubic form with space group $Fd3m\text{-}O_h^7$ [23]. It is generally know that the spinel ferrites exhibit four IR active bands, designated as υ_1, υ_2, υ_3 and υ_4. The occurrence of these four bonds have been rationalized on the basis of group theoretical calculations employing space group and point symmetric both in normal and inverse spinel. The first three IR bands are due to tetrahedral and octahedral complexes while the fourth one is due to some type of lattice vibrations. According to Waldron's classification [24], the vibration of the unit cell of cubic spinel can be constructed in the A- and B-sites, so, the high frequency absorption band υ_1, is caused by the stretching vibration of the tetrahedral metal–oxygen bond (t–O) and the low frequency absorption band υ_2 is caused by the metal–oxygen vibration in octahedral sites.

The room temperature (300 K) infrared spectrum for wet sample of $MgFe_2O_4$ is shown in Fig. 4. It can be seen that the IR spectrum of magnesium ferrite is found to exhibit two major bands in the range 400–700 cm^{-1}. The high frequency band υ_1 is centered about 625 cm^{-1} and the lower frequency band υ_2, with central frequency at 415 cm^{-1}. These bands are common features of all the ferrites [24]. The IR absorption band about 3400 cm^{-1} and weak band about 1600 cm^{-1} are assigned to stretching vibrations of bonded –OH and H–O–H of adsorbed water hydroxyl ions and 1100 cm^{-1} to sulphates ions (SO_4) while bands about 1400 cm^{-1} and 882 cm^{-1} may be due to presence of sulphone impurity present in the material.

A careful examination of IR spectrum reveals the fact that weak high frequency shoulders (υ_{sh}), high frequency (υ_1') and low frequency (υ_2') ∼402 cm^{-1} splitting occur in the IR spectrum. The high frequency shoulder is due to the disparity in the masses of Mg (24.31 amu) and Fe (55.85 amu) ions present at A-sites, while high and low frequency splitting may be due to small amount of A- and B-sites occupancy of Fe^{3+} ions in other oxidation state. The presence of Fe^{2+} ions in the ferrite can cause a splitting of the absorption band. Local deformations can occur due to Jahn–Teller effect [25] in Fe^{2+} ions which can lead to a non-cubic component of the crystal field potential and hence to splitting of the band. The distinct band observed at 680 cm^{-1} is assigned to the in-plane Fe–O–H bending vibrations [26,27]. The difference in the band position (υ_1 and υ_2) is expected because of the difference in the Fe^{3+}–O^{-2} distances for the octahedral and tetrahedral complexes. It is found by Evans and Hafner [28] that Fe–O distance of A-site (0.189 nm) is smaller than that of the B-site (0.199 nm). This can be interpreted by the stronger covalent bonding of Fe^{3+} at the A-sites than the B-sites.

The value of saturation magnetization σ_s, for wet and annealed samples of $MgFe_2O_4$ is found to be 14 emu/g and 27 emu/g, respectively at 80 K. The σ_s value of wet sample is found to be very low compared to the annealed sample. Such behaviour is attributed to surface effects and has been already observed for stoichiometric nanoparticles of Mn-ferrite [29], Mn–Zn ferrite [3] and Co-ferrite [29]. It is found through the

TGA measurement for wet sample that the net weight loss at 500 °C is 24%, the presence of water and hydroxyl ions which decreases per gram magnetization for wet sample. Thus, the lower value of σ_s for wet sample compared to annealed sample cannot be explained only on the basis of the presence of non-magnetic mass of weight loss (unknown missing mass). The missing mass can partially account for this decreasing saturation magnetization.

The acicular nanoparticles can be thought of having core–shell structure with ferrimagnetically ordered core and shell of finite and constant thickness made of weak-magnetic and non-interacting mass i.e. magnetically dead layer. The existence of the non-magnetic layer might be caused by the canting of the surface spins [30,31], a high anisotropy layer or loss of the long range order in the surface layer [32] or other reasons [28]. It has been found that this shell layer can have thickness approximately equal to one lattice constant, which means that the magnetic nature of the first crystalline layer on the nanoparticles is weakened by surface adsorption of non-magnetic ions but the magnetic properties of the core remains intact and resembles to bulk magnetization [33]. Assuming the thickness of the shell layer (t) constant the magnetization of the particles to the first order has been given by $\sigma_s^{nano} = \sigma_s^{bulk}[1 - (6t/d)]$ where, d is the particle diameter. This accounts for the almost 50% reduction in the σ_s value in case of nanoparticles compared to the bulk counterpart. Thus, in the present case the wet sample having nano-sized particles exhibits very low saturation magnetization but after annealing them at high temperature (1100 °C) the annealed sample shows expected bulk value of saturation magnetization at 80 K [34].

Thermal variation of low field (0.5 Oe) ac susceptibility curves ($\chi_T/\chi_{RT} \rightarrow T$; $\chi(T)$) depicted in Fig. 5, for wet sample, backed sample and annealed sample of $MgFe_2O_4$ exhibit differences in the shape of the $\chi(T)$ curves. The wet sample showed very weak signal for magnetic susceptibility at 300 K and showed continuous decrease of relative susceptibility on increasing temperature i.e. paramagnetic behaviour. It may be inferred that the wet sample with nano-sized particles must be having their blocking temperature (T_B) much lower than room temperature. The blocking temperature is the threshold point of thermal activation energy for whole nanoparticles sample where thermal energy (k_BT) becomes sufficient to overcome the anisotropy energy barrier. Therefore, at $T > T_B$, magnetic anisotropy is overcome by thermal activation and the magnetization direction of each nanoparticle simply follows the applied field direction. Consequently, the nanoparticles become superparamagnetic and show paramagnetic behaviour.

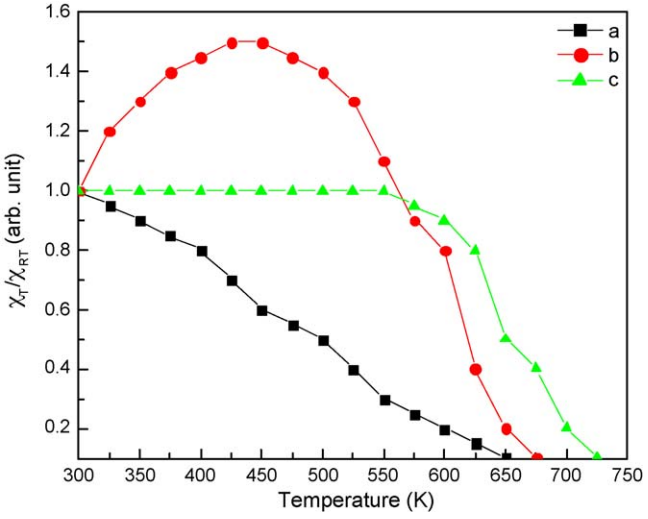

Fig. 5. Thermal variation of normalized magnetic susceptibility for wet (as prepared) (a), baked at 400 °C (b) and annealed at 1100 °C (c) samples of $MgFe_2O_4$.

The larger the particles, the higher the anisotropy energy, barrier the larger k_BT is required to become superparamagnetic. Therefore, with increasing particle size, blocking temperature also increases. Similar behaviour was observed for $CoFe_2O_4$ nanoparticles [35]. This study suggested clearly that the T_B depends upon the size of the nanoparticles and it increases as the mean diameter of the nanoparticle increases. This theory was checked for the present case by baking the as-prepared sample of $MgFe_2O_4$ at 400 °C in air thereafter, thermal variation of low field susceptibility was recorded. The change in the shape of the curve is attributed to the increase in the particle size and therefore the blocking temperature as observed in Fig. 5. If the temperature of a nano-sized acicular single domain (SD) particle is increased it may so happen that the thermal energy may become comparable to the effective magnetic anisotropy when the magnetization direction spontaneously fluctuates between the easy axes of the grain. In such state, a particle is said to be exhibiting super-paramagnetism (SP). The specific temperature at which the SD to SP transition for a particle or cluster of volume V takes place is known as the blocking temperature T_B, and the relation governing this given by: $VJ_sH_c = 2kT_B$, where J_s is the saturation intensity, H_c is the coercive force of the material and k is the Boltzman constant. For single domain particles H_c is large where as it tends to zero for SP particles. Thus, susceptibility which is inversely proportional to H_c is large for SP of the same material and hence there is peak in $\chi(T)$ curve at T_B. A broad maximum observed in $\chi(T)$ curve of baked sample may be due to the response of single domain (SD) particles of various sizes as they undergo SD to SP (superparamagnetic) transition. The $\chi(T)$ plot of annealed sample shows normal ferrimagnetic behaviour similar to that of $MgFe_2O_4$ prepared by usual double sintering ceramic technique [34]. The Neel temperature for baked sample and annealed sample is found to be 675 ± 2 K and 730 ± 2 K respectively. The Neel temperature for baked sample is found to be lower compared to annealed sample, which may be attributed to the change in the distribution of cations among the available tetrahedral (A-) and octahedral (B-) sites of spinel lattice, and/or finite size effect [28].

Room temperature (300 K), ^{57}Fe Mossbauer spectra of three specimens of $MgFe_2O_4$: wet, baked at 400 °C and annealed at 1100 °C are displayed in Fig. 6. All the spectra have been fitted using the NORMOS software. The solid line through data points are the results of computer fits of spectra obtained assuming equal line widths for A- and B-sites. The wet sample shows a paramagnetic doublet, which is due to the super-paramagnetic relaxation, that is, each particle is a single

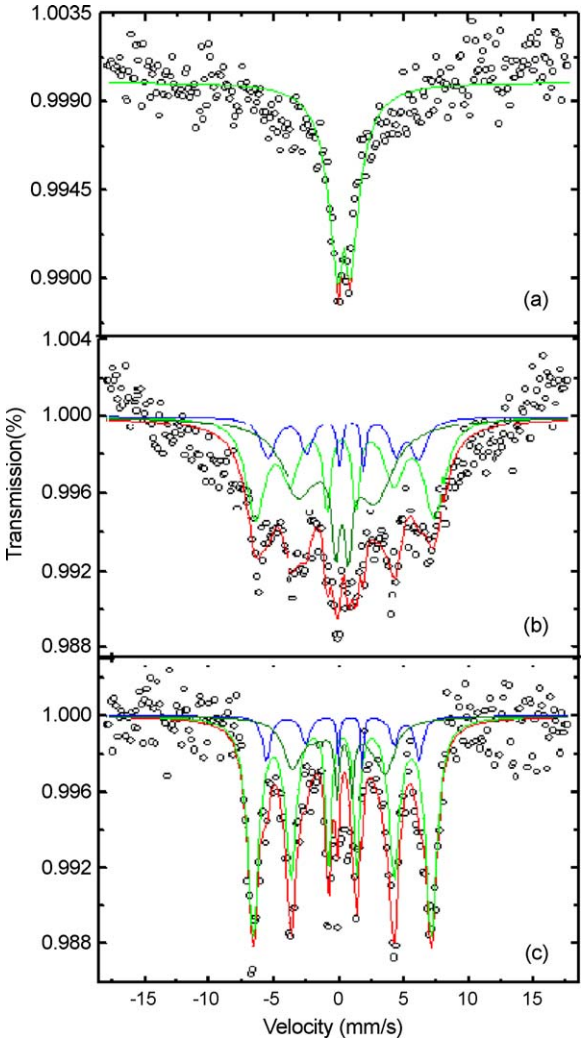

Fig. 6. Mossbauer spectra of three specimens of $MgFe_2O_4$: as prepared (a), baked at 400 °C (b) and annealed at 1100 °C (c) of $MgFe_2O_4$.

domain. These quadrupole doublets indicative of the absence of magnetic hyperfine interactions (long range ordering). This observation leads to the conclusion that in magnesium ferrite the particles have a very fine size or more probably these ferrimagnetic nanoparticles are separated magnetically from the matrix since the region is surrounded by non-magnetic Mg^{2+}-ions. Thus, the Mossbauer spectrum of as prepared sample reveals the existence of SP clusters or paramagnetic centers [36]. This indicates that ferrimagnetic wet sample is superparamagnetic at 300 K, their blocking temperature being lower than the room temperature as observe in $\chi(T)$ measurement.

Recalling the core–shell structure of the nanoparticles, a different environment is experienced by Fe atoms residing in the shell compared to those inside the core. The broad doublet is therefore fitted with two sets of doublet corresponding to the quadrupole splitting (Q.S.) of the iron nucleus in the shell (surface region) and the core region of the particle. It is deduced from the area ratio of the doublets that the contribution from the sell region atoms is 23%, which is agreeing to the reduction in saturation magnetization for as-prepared sample. The QS in the shell region (0.48 ± 0.02 mm/s) is much larger than the QS in the core region (0.26 ± 0.02 mm/s). This is ascribed to the disorder and reduction in the local symmetry of the Fe atom in the shell region of the nanoparticle. The Mossbauer spectrum of baked sample exhibits simultaneous presence of a central paramagnetic doublet superimposed on broad magnetic sextet, indicating the partial transformation to an ordered magnetic structure. The Mossbauer spectrum of annealed sample shows two well resolved Zeeman split sextets corresponding to A- and B-sites Fe^{3+}-ions with nuclear hyperfine fields 480 ± 1 kOe and 510 ± 1 kOe respectively. The magnetic phase change of the ferrite particles is attributed to the change in particle size as a function of heat treatment employed.

4. Conclusions

The nanoparticles of $MgFe_2O_4$ have been successfully synthesized by a co-precipitation technique. TEM analysis reveals the fact that the obtained ferrite particles are thick needle-shaped nanocrystals with an aspect ratio of around 3.5 and long axis of 37 nm. This is due to collective role of NaOH, H_2O_2 and Mg^{2+} in governing the rate of growth of growing planes of nanocrystals. We have established that the wet chemically prepared magnesium ferrite contain nanoparticles which give rise to the unusual magnetic properties like super-paramagnetism leading to the suppression of long range magnetic ordering and quenching of magnetic moments in spite of having Neel temperature > 700 K, in annealed state. The lower value of saturation magnetization for as-prepared nanopowder can be explained on the basis of core–shell structure and surface effects corroborated by Mossbauer spectral signature. Mossbauer spectral and susceptibility studies showed that the as-prepared nano-sized ferrite is superparamagnetic at room temperature and magnetic ordering evolves on baking and annealing the nanopowdered sample due to increase in the crystalline size. The high temperature annealing transforms the nanostructured ferrite to coarse-grained ceramic ferrite powder.

In IR spectrum, the weak high frequency shoulder is due to the disparity in the masses of cations present at A-sites, while high and low frequency splitting may be due to small amount of A- and B-sites occupancy of Fe^{3+} ions in other oxidation state. Local deformation can occur due to Jahn–Teller effect in Fe^{2+} ions which can lead to a non-cubic component of the crystal field potential and hence to splitting of the bands.

Acknowledgements

Authors are thankful to Prof. H.H. Joshi and Dr. G.J. Baldha for fruitful discussion and Ms. Pooja Sharma, Mr. Arvind Chavda and Ms. Bhakti Desai for their help in data collection and analysis. One of the authors (KBM) is thankful to UGC-New Delhi for providing financial assistance under UGC research award - 2009.

References

[1] C.C. Koch, Synthesis of nanostructured materials by mechanical milling: problems and opportunities, Nanostruct. Mater. 9 (1–8) (1997) 13–22.

[2] T.K. Pathak, J.J.U. Buch, U.N. Trivedi, H.H. Joshi, K.B. Modi, Infrared spectroscopy and elastic properties of nanocrystalline Mg–Mn ferrites prepared by co-precipitation technique, J. Nanosci. Nanotech. 8 (8) (2008) 4181–4187.

[3] K. Parikh, R.V. Upadhyay, L. Belova, K.V. Rao, Ternary monodispersed $Mn_{0.5}Zn_{0.5}Fe_2O_4$ ferrite nanoparticles: preparation and magnetic characterization, Nanotechnology 17 (2006) 5970–5975.

[4] X. Cao, L. Gu, Spindly cobalt ferrite nanocrystals: preparation, characterization and magnetic properties, Nanotechnology 16 (2005) 180–185.

[5] P.P. Hankare, V.T. Vader, N.M. Patil, S.D. Jadhav, U.B. Sankpal, U.B. Kadam, B.K. Chougle, N.S. Gajbhiye, Synthesis, characterization and studies on magnetic and electrical properties of Mg ferrite with Cr substitution, Mater. Chem. Phys. 113 (1) (2009) 233–238.

[6] S. Thaker, S.C. Katyal, M. Singh, Structural and magnetic properties of nano nickel–zinc ferrite synthesized by reverse micelle technique, J. Magn. Magn. Mater. 113 (1) (2009) 1–7.

[7] Y.P. Fu, C.H. Lin, Microwave-induced combustion synthesis of $Li_{0.5}Fe_{2.5-x}Mg_xO_4$ powder and their characterization, J. Appl. Phys. 105 (7) (2009) 07a5051-3.

[8] Y. Li, M. Sui, Y. Ding, G. Zhang, J. Zhuang, C. Wang, Preparation of $Mg(OH)_2$ nanorods, Adv. Mater. 12 (2000) 818–821.

[9] S. Vladimir, et al., Magnetic properties of nanostructured MnZn ferrite, J. Magn. Magn. Mater. 321 (3) (2009) 152–156.

[10] N. Shivakumar, D. Narayanasamy, N. Ponpandian, G. Govindraj, Grain size effect on the dielectric behavior of nanostructured $Ni_{0.5}Zn_{0.5}Fe_2O_4$, J. Appl. Phys. 101 (8) (2007) 0841161-6.

[11] C.N. Chinnasamy, A. Narayanasamy, N. Ponpandian, K. Chattopadhyay, K. Shinoda, B. Jeyadevan, K. Tohji, K. Nakatsuka, T. Furubayashi, I. Nakatani, Mixed spinel structure in nanocrystalline $NiFe_2O_4$, Phys. Rev. B 63 (18) (2001) 184108–184113.

[12] M. Ozaki, T. Egami, N. Sugiyama, E. Matijevic, Agglomeration in colloidal hematite dispersions due to weak magnetic interactions. II. The effects of particle size and shape, J. Colloid Interf. Sci. 126 (1988) 212–219.

[13] M. Ozaki, H. Suzuki, K. Takahashi, E. Matijevic, Reversible ordered agglomeration of hematite particles due to weak magnetic interactions, J. Colloid Interf. Sci. 113 (1986) 76–80.

[14] J. Lv, L. Qiu, B. Qu, Controlled synthesis of magnesium hydroxide nanoparticles with different morphological structures and related properties in flame retardant ethylene–vinyl acetate blends, Nanotechnology 15 (2004) 1576–1581.

[15] C. Radhakrishnamurthy, S.D. Likhite, P.W. Sahasrabudhe, In situ measurements on igneous rock bodies, Proc. Ind. Acad. Sci. A 87 (1978) 245–249.

[16] C. Radhakrishnamurthy, S.D. Likhite, Hopkinson effect, blocking temperature and Curie point in basalts Earth Planet, Sci. Lett. 7 (5) (1970) 389–396.

[17] B.D. Cullity, Elements of X-ray diffraction, 2nd edn., Addison Wesley Pub. Co., Reading, MA, 1978.

[18] J. Moon, M. Awano, H. Takaji, Y. Fujishiro, Synthesis of nanocrystalline manganese oxide powders: influence of hydrogen peroxide on particle characteristics, J. Mater. Res. 14 (12) (1990) 4594–4601.

[19] D.D. Khunti, M. Phil. Dissertation, Saurashtra University, Rajkot, India, 2008.

[20] S. Manickam, et al., Fabrication of zinc ferrite nanocrystals by sonochemical emulsification and evaporation: observation of magnetization and its relaxation at low temperature, J. Phys. Chem. B 110 (31) (2006) 15234–15243.

[21] J.M. Petrovski, T.C. Green, M.A. El-Sayed, Self-assembly of platinum nanoparticles of various size and shape, J. Phys. Chem. A 105 (23) (2001) 5542–5547.

[22] Z.L. Wang, Transmission electron microscopy of shape-controlled nanocrystals and their assemblies, J. Phys. Chem. B 104 (2000) 1153–1175.

[23] W.B. White, B.A. de Angelis, Interpretation of the vibrational spectra of spinels, Spectrochim. Acta 23 (4) (1967) 985–995.

[24] R.D. Waldron, Infrared spectra of ferrites, Phys. Rev. B 99 (6) (1955) 1727–1735.

[25] V.A. Potakova, N.D. Zvery, V. Ramanov, On the cation distribution in $Ni_{1-x-y}Fe_x^{2+}Zn_yFe_2^{3+}O_4$ spinel ferrites, Phys. Stat. Sol. (a) 12 (2) (1972) 623–627.

[26] J. Gir, T. Sriharsha, D. Bahadur, Optimization of parameters for the synthesis of nano-sized $Co_{1-x}Zn_xFe_2O_4$, ($0 \leq x \leq 0.8$) by microwave refluxing, J. Mater. Chem. 14 (2004) 875–890.

[27] C. Sudakar, G.N. Subbana, T.R.N. Kutty, Synthesis of acicular hydrogoethite (α-FeOOH·xH_2O; 0. $1 < x < 0.22$) particles using morphology controlling cationic additives and magnetic properties of maghemite derived from hydrogoethite, J. Mater. Chem. 12 (2002) 107–116.

[28] B.J. Evans, S. Hafner, Mössbauer resonance of Fe^{57} in oxidic spinels containing Cu and Fe, J. Phys. Chem. Solids. 29 (9) (1968) 1573–1588.

[29] L.D. Tung, V. Kulesnichenko, D. Caruntu, N.H. Chou, C.J. O'connor, L. Spinu, Magnetic properties of ultrafine cobalt ferrite particles, J. Appl. Phys. 9 (10) (2003) 7486–7488 (and references there in).

[30] J.M.D. Coey, Noncollinear spin arrangement in ultrafine ferrimagnetic crystallites, Phys. Rev. Lett. 27 (17) (1971) 1140–1142.

[31] A.H. Morrish, K. Haneda, P.J. Schiurer, Surface magnetic structure of small γ-Fe_2O_3 particles, J. Phys. C 37 (1971) 301–305.

[32] A.E. Berkowitz, J.L. Walter, Amorphous particles produced by spark erosion, Mater. Sci. Eng. 55 (2) (1982) 275–287.

[33] Z.X. Tang, C.M. Srensen, Klabunde, G.C. Hadjipanayis, Size-dependent curie temperature in nanoscale $MnFe_2O_4$ particles, Phys. Rev. Lett. 67 (25) (1991) 3602–3605.

[34] K.B. Modi, H.H. Joshi, R.G. Kulkarni, Magnetic and electrical properties of Al^{3+}-substituted $MgFe_2O_4$, J. Mater. Sci. 31 (5) (1996) 1311–1317.

[35] Chao Liu, A.J. Rondinone, Z. Zhang, Synthesis of magnetic spinel ferrite $CoFe_2O_4$ nanoparticles from ferric salt and characterization of the size-dependent superparamagnetic properties, J. Pure Appl. Chem. 72 (1–2) (2000) 37–45.

[36] Y. Ishikawa, Superparamagnetism in magnetically dilute systems, J. Appl. Phys. 35 (30) (1964) 1054–1059.